Int J Fract (2020) 226:233–242
https://doi.org/10.1007/s10704-020-00490-y

ORIGINAL PAPER

Non-monotonic precursory signals to multi-scale catastrophic failures

Hu Wang · Sheng-Wang Hao · Derek Elsworth

Received: 20 July 2020 / Accepted: 26 September 2020 / Published online: 22 October 2020

Abstract Identifying precursory trends in acoustic/seismic observations allows the forewarning/prediction of catastrophic events. However, rupturing across multiple scales leaves it unclear whether features of small events are applicable predictors of the larger ensemble final collapse. To resolve this issue, we present a multiscale heterogeneous model that straightforwardly characterizes the duration and mechanism of multiscale catastrophic failures. Our results identify four distinct classes of failure including random single breaks, small catastrophic failure (SCF) events, large catastrophic failure (LCF) events that consist of subordinate SCF and random break events, and a culminating macroscopic catastrophic failure (MCF) event resulting from the coalescence of subordinate LCF events. Only the local response quantities, recorded at their corresponding position, show an accelerating precursory trend to an SCF event. LCF events can appear in stages both before and after the maximum load in the system. Our findings highlight that although cumulative LCF event and deformation rates for the entire system always exhibit singular accelerating precursors as MCF is approached, this is not true at all individual event points. This may explain why no clearly accelerating precursor is observed before some catastrophic events. Thus, these results suggest a methodology for recognizing and distinguishing effective precursory information from monitoring signals across scales and in eliminating false predictions.

Keywords Catastrophic failure · Multi-scale events · Precursory signals · Non-monotonic · Prediction of failure · Heterogeneous materials

H. Wang · S.-W. Hao (✉)
School of Civil Engineering and Mechanics, Hebei Provincial Key Laboratory of Green Construction and Intelligent Maintenance of Civil Engineering, Yanshan University, Qinhuangdao, China
e-mail: hsw@ysu.edu.cn

D. Elsworth
Energy and Mineral Engineering, Geosciences, G3 Center, and EMS Energy Institute, Pennsylvania State University, University Park, PA, USA

1 Introduction

Catastrophic failure in heterogeneous materials has attracted substantial interest (Kilburn and Petley 2003; Main and Naylor 2012; Heap et al. 2011; Hao et al. 2014; Sornette 2002) due to its relevance to a broad array of engineered and natural systems. These include phenomena spanning structures in civil, mechanical, marine, aeronautics and astronautics engineering and processes in natural hazards including earthquakes, volcanic eruptions, landslides and avalanches. Heterogeneities at different scales result in a broad spectrum of complex failure behaviors (Sornette 2002; Kilburn 2003; Zapperi et al. 1997; Vasseur et al. 2015, 2017; Kadar and Kun 2019) making prediction of failure difficult. Conversely, this high degrees of heterogeneity and resulting disorder in materials may produce a cumulative trend in damage as failure is approached

with distinct features—thereby offering a unique signature of precursory phenomena (Sornette 2002; Kilburn 2003; Vasseur et al. 2017; Kadar and Kun 2019; Mogi 1995; Hao et al. 2017a, b). Evolution towards a macroscopic catastrophic event may comprise multiple physical processes at different scales and their possible interdependences. Therefore, faithful representation of the multi-scale nature of failure in heterogeneous materials is crucial for our understanding of rupture and in failure prediction (Kilburn 2003; Zapperi et al. 1997; Vasseur et al. 2015). However, the specific connection of a large culminating event to the contributory smaller scale events remains unclear. This creates a challenge in identifying representative signals that are precursory to the impending catastrophic event.

Analyzing the precursors to catastrophic failure is a long-standing problem—although approaches have been codified and widely used to predict material failures. Typically, acceleration in "response quantities", such as accumulative seismic events, acoustic emissions or deformations, as catastrophic failure is approached, are used in the field monitoring of volcanic eruptions (Cornelius and Voight 1995; Voight and Cornelius 1991; Kilburn and Voight 1998), landslides (Kilburn 2003; Petley et al. 2005), earthquakes and in laboratory experiments (Heap et al. 2011; Hao et al. 2014; Nechad et al. 2005; Hao et al. 2017a, b; Voight 1989). This accelerating process can be described by Voight's relation (Voight 1988, 1989; Cornelius and Scott 1993) and presents a power law relationship (Voight 1988, 1989; Kilburn and Voight 1998; Petley et al. 2005; Hao et al. 2014; Nechad et al. 2005; Hao et al. 2017a, b; Cornelius and Scott 1993; Main 1999, 2000; Turcotte et al. 2003; Bell et al. 2011; Boué et al. 2015; Zhou et al. 2018) with respect to time-to-failure. The emergence of Voight's relation may be explained by applying statistical mechanics to rock fracture (Kilburn 2003, 2012) and to extend analyses to deformation under a changing stress regime (Kilburn 2012). Such a power law relation can be expressed as the relative change in response quantities (Kilburn 2012; Hao et al. 2017a, b) with respect to the controlling load variable of stress (Kilburn 2012; Hao et al. 2016) or boundary displacement (Hao et al. 2013, 2017; Xue et al. 2018). But this form of accelerating precursor is not always observed before some catastrophic failure events. The cause for the absence of this accelerating precursor remains unclear.

Macroscopic fractures grow from the coalescence of micro-cracks. Cracks at all scales propagate unstably where the energy released from the surrounding mass exceeds that required for nucleation and propagation (Griffith 1921). Elastic energy release is a fundamental mechanism contributing to dynamic and unstable failure with short-warning-times such as the failure of structures in rock (Salamon 1970; Jaeger et al. 2007) and abrupt failure of specimens tested in the laboratory (Hao et al. 2013, 2014; Xue et al. 2018). This intrinsic mechanism results in failures cascading over a spectrum of scales when the local energy release rate drives the response. However, the cross-scale relationships of these catastrophic events remain unclear.

Acoustic emissions (AE) or seismic events implicated in macroscopic failure evolve across a spectrum of length- and time-scales. Recognizing their multi-scale evolution and precursory signatures is essential for improving time-to-failure warnings (Kilburn et al. 2018). Models must anticipate potential oscillations in seismic event rates and identify that local peaks in local event rate (i.e., the inverse-rate minima), rather than all seismic events, play a key indicator in approaching failure (Kilburn 2003). This global predictive method has been validated against field (Kilburn 2003) and laboratory observations (Lavallée et al. 2008). However, an underlying unresolved issue is in determining what scale of smaller events are directly related to larger or culminating catastrophic events - i.e. what scale of small events are suitably precursory to a larger event.

Based on the intrinsic mechanism of energy release driving catastrophic failure, we develop a multi-scale model to address this issue of event size consistency. The model consists of elastic springs and damageable links in a variety of configurations. This model provides direct illustration of mechanisms and signatures of multi-scale catastrophic failures. Energy release from the elastic springs when far-from-overall-failure results in small catastrophic failure in some distributed meso-elements. Energy release from the elastic springs at two scales drives a large catastrophic event that involves random distributed breaks and smaller catastrophic events. Macroscopic catastrophic failure occurs when such cumulative events coalesce in space and time. Our findings show that event size grows as the system accelerates to macroscopic catastrophic failure, but local cumulative counts do not necessarily show this critical trend. The smaller breaks in a local meso-element

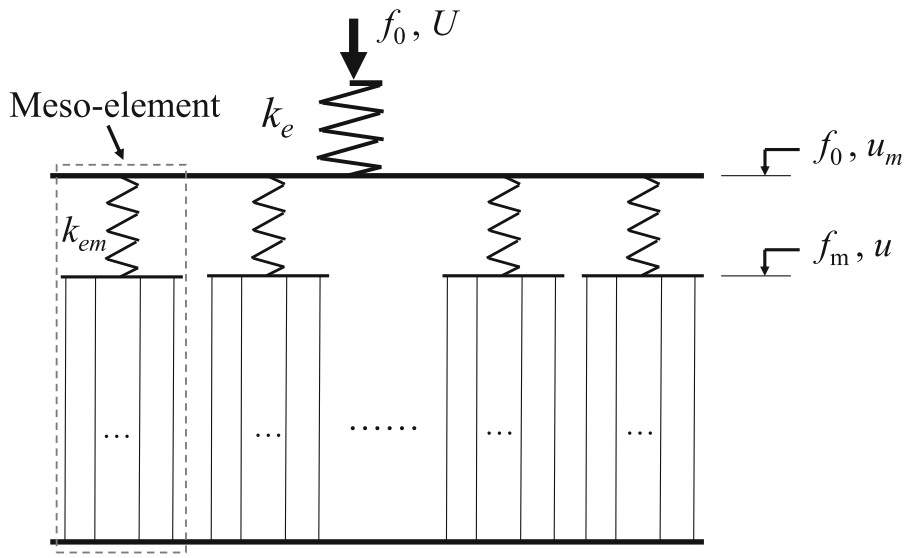

Fig. 1 Multi-scale system consisting of a primary elastic spring with a stiffness of k_e and a sub-system in series. The sub-system comprises multiple meso-elements in parallel. Each meso-element combines an elastic spring with a stiffness of k_{em} in series with a fiber bundle of many parallel and breakable fibers

only play a precursory signal to local small catastrophic failure.

2 Multi-scale model and numerical calculations

To demonstrate the occurrence of multi-scale catastrophic failures driven by energy release, we focus on a system consisting of a linear elastic spring and a sub-system in series as shown in Fig. 1. The sub-system comprises M meso-elements in parallel. Each meso-element consists of a linear elastic spring and N_m damageable links in series. The damageable links are elastic-brittle fiber bundles and represent a class of simple models widely used (Peirce 1926; Sornette 1989; Duxbury et al. 1995; Hidalgo et al. 2002; Pradhan et al. 2010; Kun et al. 2003; Moreno et al. 2000) to explain evolving failure mechanisms in heterogeneous materials— and proven effective in the study of failure process of disordered materials (Hao et al. 2016, Hao et al. 2017a, Hao et al. 2017b; Hidalgo et al. 2002; Pradhan et al. 2010; Kun et al. 2003; Moreno et al. 2000). Specifically in this work, we build a multi-scale system with heterogeneities at different scales representing heterogeneous elastic environments at different spatial positions and at different scales. The boundary displacement U of the macro-system is the sum of the uniform deformation u_m of the sub-system and the deformation of the primary elastic spring with a stiffness of k_e (Fig. 1).

A global load-sharing criterion is chosen for the redistribution of load following a break in the meso-element fibers. All the fibers are linearly elastic and assumed to have the same stiffness until they break. A fiber breaks when it reaches its strength— subsequently it carries no load. The surviving fibers in a meso-element equally share the force released by the broken fibers. All meso-elements share the load according to their stiffness ratio with respect to the total stiffness of the sub-system. A meso-element no longer carries load when it has no surviving fibers.

The stiffness of a single fiber is assumed to be unity. Then, the normalized force (f)-deformation (u) response of an unbroken fiber has the relationship $f = u$. The nominal force in each meso-element is then $f_m = f(N_m - N_{bm})/N_m$ where N_{bm} is the number of broken fibers in the meso-element. As a consequence, the nominal force is $f_0 = \sum_{m=1}^{M} f_m/M$ on the macroscopic system with M meso-elements and the total number of broken fibers $N_b = \sum_{m=1}^{M} N_{bm}$ is the sum of those in all meso-elements.

The strength of fibers in each meso-element is assumed to follow the Weibull distribution $P(f_{th}) = 1 - \exp[-(f_{th}/\eta)^{\theta}]$. In order to describe the heterogeneity among meso-elements, parameters η and θ are different among meso-elements and follow the Weibull distribution $P(\eta) = 1 - \exp(-\eta^{\gamma})$ for η and a uniform distribution ranging from 2.0 to 6.0 for θ.

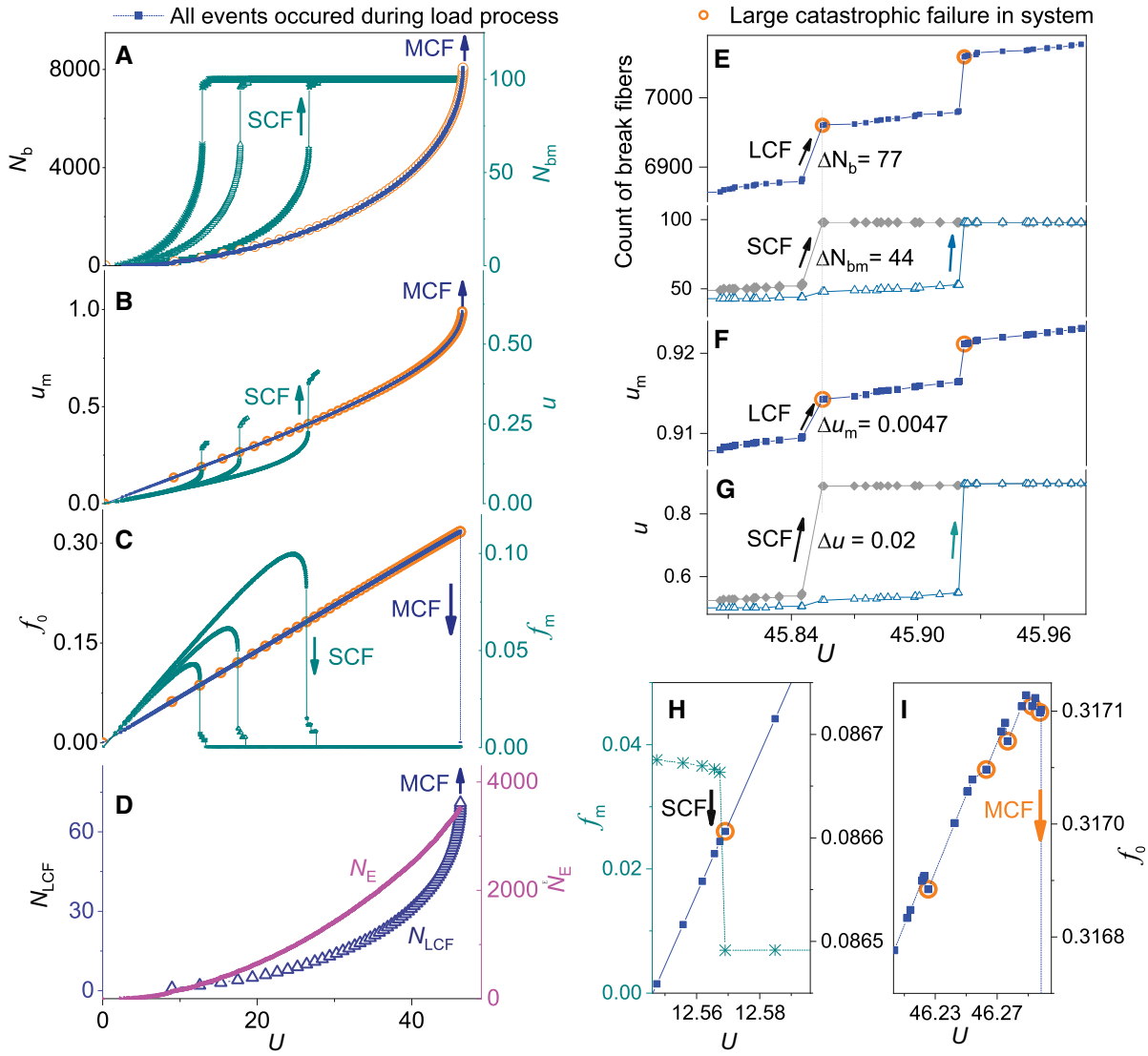

Fig. 2 Evolution of catastrophic failure across different scales. **a** Evolution of breakage of fibers. **b** u_m (u) vs U. **c** Evolution of force vs U. Evolution in the response of three representative meso-elements is shown to illustrate small-catastrophic-failure (SCF) occurring in the meso-elements. **d** Cumulative number of events (N_e, N_{LCF}) vs U. **e**, **f**, **g**, **h**, **i**). Zoom-in of LCF events showing their relationship with, and differences from, SCF events. Gray solid diamonds and empty triangles in subplots E, F and G represent typical evolution (N_{bm} and u versus U) curves of two meso-elements, respectively, where SCF events occur The total number of meso-elements in the simulations is M =200 and the number of fibers in each meso-element is N_m =100

In order to represent multi-scale accelerating failures, Monte Carlo simulations of the failure process are performed. In these calculations, the stiffness of the primary elastic spring connected to the sub-system is set to 1.4 N_m since every fiber has a unit stiffness, and the stiffnesses of elastic springs in the meso-elements follow a uniform distribution ranging from 0.4 N_m to 1.4 N_m. The load process is driven as the boundary displacement U is monotonically increased at a sufficiently slow rate that the breaking fibers increase to produce a smallest positive increment of U at each calculation step.

The calculation sequence proceeds as follows: Let fibers break one by one, i.e. every time let only a single

fiber break that requires the minimum increment of the boundary displacement. Thus, when one fiber breaks in a meso-element, all other meso-elements deform elastically because no additional fibers break within them. When a fiber with a strength of f_{im} (u_{im} represents the corresponding deformation of this fiber) in a meso-element breaks, then the load supported by this meso-element becomes $f_{im}(N_m - N_{bm})$ and its deformation is $u_m = f_{im}(N_m - N_{bm})/k_{em} + u_{im}$. Then the deformations of other meso-elements are identically determined as u_{m} based on their geometric relationship of parallel connection shown in Fig. 1, and their forces can be calculated through the elastic force-deformation relationship. The nominal force f_0 and the boundary displacement U on the system are correspondingly calculated. After some meso-elements transit to their post-peak force, the decrease in the load supported by a meso-element due to an internal fiber-break may result in a decrease in the resultant nominal force on the system, and thus the primary elastic spring unloads and releases its deformation energy. Thus, this fiber break could result in a negative increment in the boundary displacement. Subsequently, we will find the next fiber that requires the minimum increment (may be negative or positive) of the boundary displacement and let it break. We repeat this process until the resultant increment of the boundary deformation in this step ΔU is larger than zero. This progressive breaking process of fibers builds towards an intermediate catastrophic failure event—at which this load step is complete. This calculation cycle is repeated until the system fails in its entirety. This method follows the failure process and is used to understand signatures of discernable failure signals.

3 Results of multiscale catastrophic failure events

Figure 2 shows calculated results for the response quantities with respect to the control variable of system displacement U. Response quantities include: the deformation of the sub-system u_{m}, number of broken fibers N_{b}, breakage event counts N_{E}, and others. With a monotonic increase in system displacement, U, four kinds of break events spontaneously appear at different scales. These include the random breakage of a single fiber, and what we classify as small catastrophic failure (SCF) events (occurring in meso-elements), a large catastrophic failure (LCF) events (occurring in the system) and macroscopic catastrophic failure (MCF) events (leading to the overall failure of the system). The energy release of the elastic spring in a meso-system induces an SCF event (Fig. 2a), and correspondingly a jump in deformation u (Fig. 2b) and force f_{m} (Fig. 2c) in the fiber bundle.

Every LCF event combines an SCF event in one meso-element and some distributed breaking of fibers in other meso-elements that is driven by energy release of the primary spring connected to the sub-system. Thus, an LCF event could result in the breaking of more fibers than the SCF event (see Fig. 2e). An example shown in Fig. 2f and g illustrates that an SCF event leads to a large jump (Δu) in deformation of the fiber bundle but a much lower increment (Δu_{m}) in deformation of a meso-element. An LCF event only induces a small fluctuation in the global trend of the force displacement curve (Fig. 2c, h and i).

LCF events show a clearly cumulative trend with increasing U, i.e. in approaching an MCF event the frequency of LCF events increases (Fig. 2a–c). This trend can be further directly observed in the curve of N_{LCF} vs U illustrated in Fig. 2d.

The normalized break rate $\Delta N_{\mathrm{b}}/\Delta U$ of fibers (Fig. 3a), and deformation $\Delta u_{\mathrm{m}}/\Delta U$, and event rates $\Delta N_{\mathrm{E}}/\Delta U$ (Fig. 3c) do not show accelerating trends when they approaches the MCF event. N_{E} represents the cumulative number of all events, including both LCF events and random breaking of fibers between two LCF events with a monotonic increase in U. However, the LCF event rate ($\Delta N_{\mathrm{LCF}}/\Delta U$) shows a clear accelerating trend as the MCF event is approached (Fig. 3d). The deformation rate ($\Delta u_{\mathrm{LCF}}/\Delta U$) recorded at the occurrence of the LCF events also presents a similar accelerating trend (Fig. 3e).

The linear parts of the log-log plots (Fig. 4) of the LCF event rate ($\Delta N_{\mathrm{LCF}}/\Delta U$) and deformation rate ($\Delta u_{\mathrm{LCF}}/\Delta U$) relative to progressive deformation (U_{F}-U) show that these two rates can be well described using a power law relationship

$$\Delta R/\Delta U \sim (U_{\mathrm{F}} - U)^{-\beta} \tag{1}$$

where R represents the cumulative response quantities of N_{LCF} and u_{LCF}. The fitted exponents of β are $\sim$0.5 for $\Delta u_{\mathrm{LCF}}/\Delta U$ and $\sim$0.55 for $\Delta N_{\mathrm{LCF}}/\Delta U$. These imply that the accelerating precursory trend to an MCF event could be hidden by the small events occurring between LCF events if all events are indeed recorded.

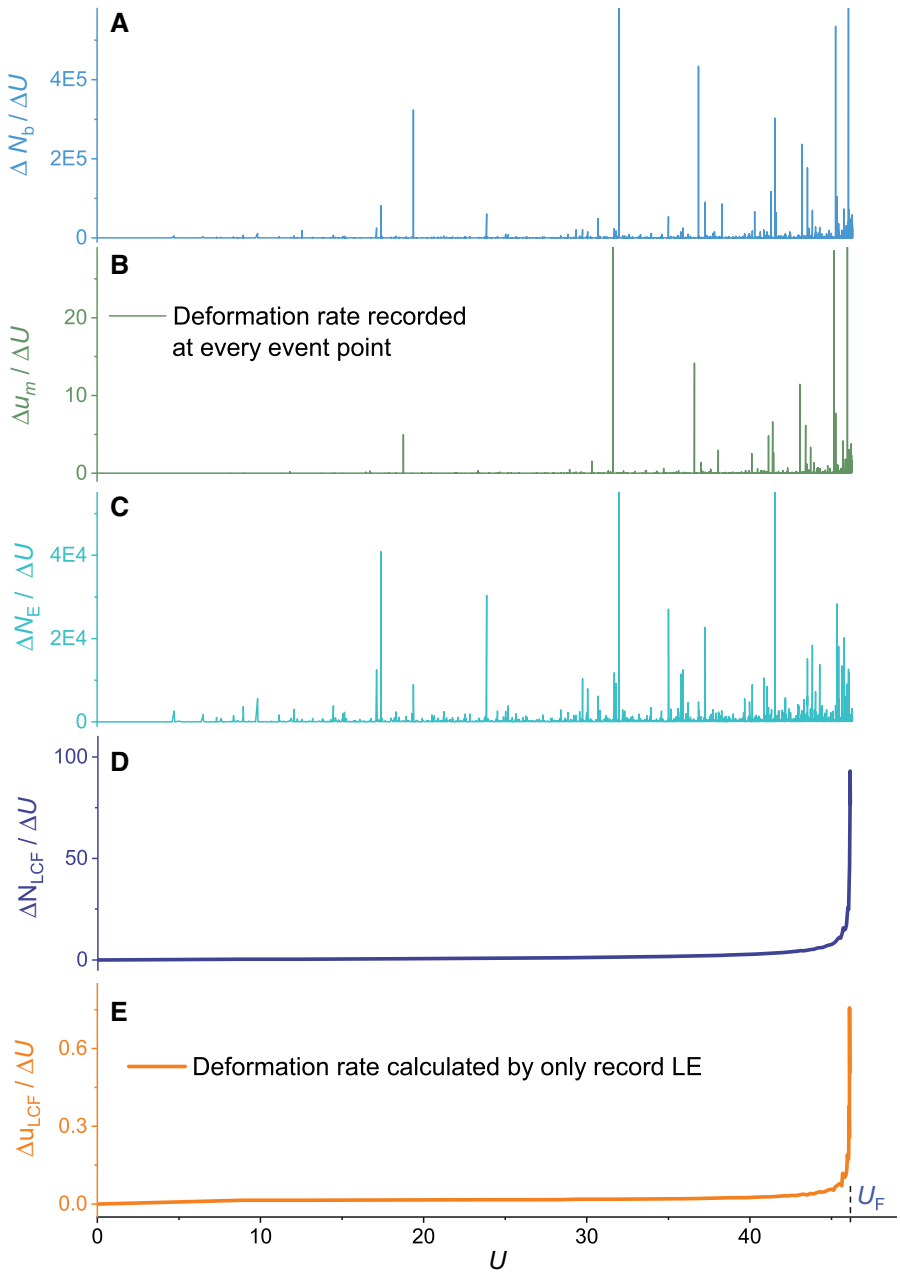

Fig. 3 Rate of change in response quantities for monotonically increasing U. **a** Break-rate of fibers, **b** Deformation-rate recorded at each event point. **c** Event-rate. **d** LCF event-rate. **e** Deformation-rate recorded only at LCF event points

The initiation of a volcanic eruption may be viewed as prompted by the movement of magma to the surface. This occurs by developing a fluid transmissive network by extending then linking pre-existing fractures progressively along the axial cylinder representing the evolving magmatic conduit – and opening a pathway for magma to reach the surface. Each fracture itself has a process zone containing smaller cracks. A cycle of growth and coalescence among the smaller cracks in the process zone of a fracture leads to oscillations in monitored seismic event rate with time (Kilburn 2003). Thus, the rate of increase in peak event rate (rather than all seismic events) is suggested as a key indicator of the approach to eruption (Kilburn 2003). Similarly, rheological experiments with continuous microseismic monitoring have shown that peaks in the event rate best predict the path to failure (Lavallée et al. 2008).

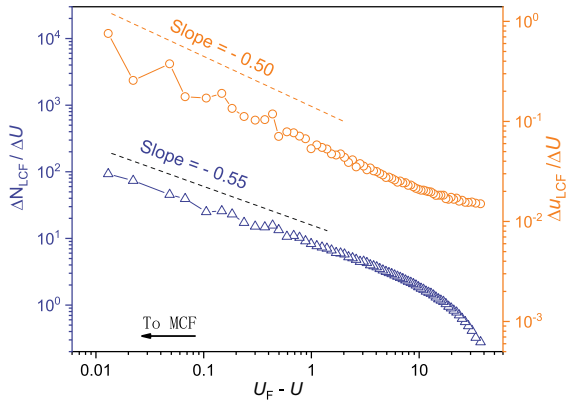

Fig. 4 Power law singularity trends for cumulative LCF events as MCF is approached

4 Mechanism of multi-scale catastrophic failures and accelerating singularity precursors

The geometric condition of a meso-element gives that the increment of displacement is the sum of the deformation increment of the spring Δu_{em} and that of the fiber bundle Δu in this meso-element, as,

$$\Delta u_m = \Delta u_{em} + \Delta u \quad (2)$$

When this meso-element transits to its post-peak force stage, the spring within it unloads and recovers its deformation, and thus Δu_{em} becomes negative. When the deformation recovery of the spring is sufficient to compensate for the necessary deformation Δu driving the breaking of fibers in a meso-element, the total deformation u_m of this meso-element decreases.

Figure 5 illustrates the analytical results of the complete curves of u versus u_m and f_m versus u_m (u) for an ideal continuous case with an infinite number of fibers where the deformation u of the fiber bundle is monotonically increased. Alternatively, if the load-controlling variable is changed to the total deformation u_m of this meso-element, the monotonically continuous increase of u_m will induce a discontinuous jump of u and the number of breaking fibers along the tangent direction (vertical direction) from point C to D as shown in Fig. 5a, i.e., a catastrophic failure (an SCF event). This results in a discontinuous jump in the curve of f_m versus u along the tangent line with a slope of $-k_{em}$ (Fig. 5b). At the point of incipient catastrophic failure, an infinitesimal increment of u_m results in a finite increment of u and a serial breaking of fibers from C to D, i.e. $(du/du_m)_c \to \infty$ (Fig. 5a)—and $(df_m/du_m)_c \to \infty$ for the f_m versus u_m curve (Fig. 5b). Thus, the mechanism of catastrophic failure determines the accelerating singularity precursor.

Similarly, the geometric condition of the macroscopic system gives that

$$\Delta U = \Delta u_m + \Delta u_e \quad (3)$$

where Δu_e is the deformation increment of the primary elastic spring connected to the sub-system. When the required deformation increment Δu_m resulting in an SCF event is larger than the deformation recovery of the primary elastic spring, the macro-system is stable and only an SCF event appears in a meso-element. Then the global force-deformation (f_0 vs U) curve is smooth and continuous as shown in Fig. 2h but a small oscillation

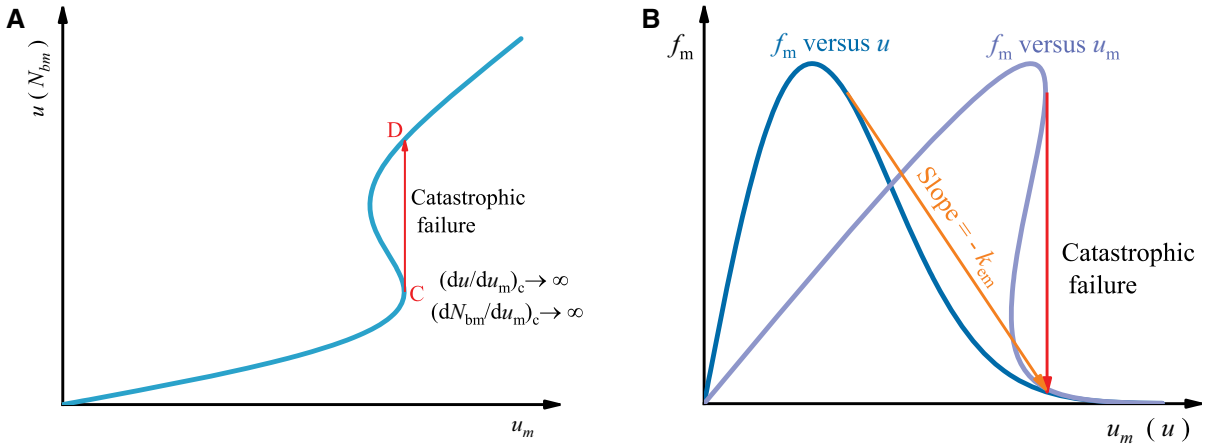

Fig. 5 Analytical results of complete curves for an ideal continuous case when m = 2, k = 0.3. **a** u (N_{bm}) versus u_m, B) f_m versus u_m (u). This illustrates the mechanism of catastrophic failure that hosts the precursor accelerating to a singularity

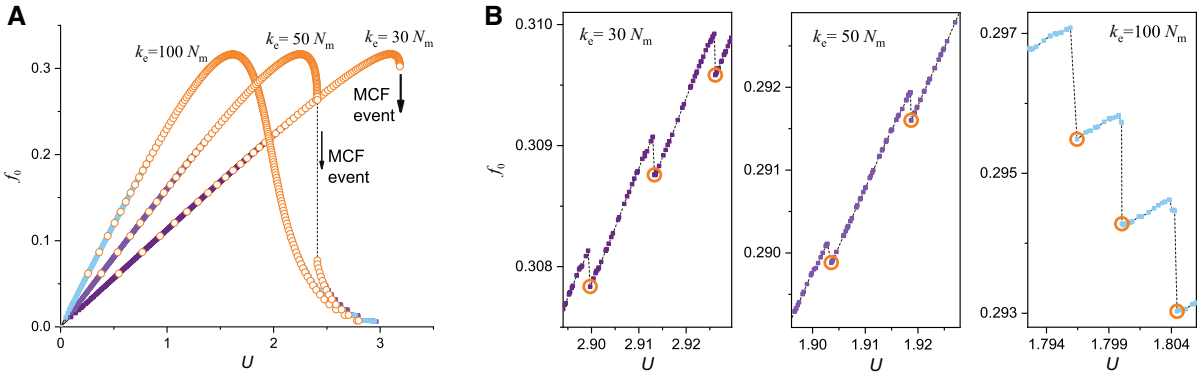

Fig. 6 Nominal force vs. boundary displacement for the primary elastic spring with different stiffness ratios. **a** Complete curves. **b** Zoom-in to show LCF events inducing discontinuity in the force-displacement curves. Scatter yellow circles in symbols represent the response quantities recorded at LCF events

occurs in the u_m vs U curve. For this case, an LCF event only includes an SCF event. Otherwise, an increment of ΔU will lead to the distributed random breaking of fibers in other meso-elements in addition to an SCF event (e.g. the case shown in Fig. 2e and f). This LCF event leads to a discontinuity of the evolving form of f_0 versus U(Fig. 2i). This LCF event is a combined result of energy release from both the spring connected to sub-system and the spring within a meso-element. LCF events can appear both before and after the point of maximum load (Fig. 2i).

Based on statistical theory describing the evolution of mesoscopic defects, the damage-failure transition is considered (Naimark 2004, 2017; Naimark and Uvarov 2004) as a specific type of critical phenomena of structural scaling transitions that could result in kind of catastrophic events mentioned in this paper. In their model, the transition is related to collective modes of damage localization that is responsible for the nonlinear properties of the free energy release rate under dynamic and shock wave loading (Naimark 2004, 2017; Naimark and Uvarov 2004).

When energy release from the primary elastic spring is sufficient to induce more than a single LCF event, it leads to the coalescence of LCF events and thus an MCF event. The stiffness of the elastic spring determines its deformation recovery rate and energy release rate. Figure 6 shows results when the stiffness ratio of the primary elastic spring has other values. When it is larger than the maximum negative value of the slope of the force–deformation curve of the sub-system recorded at LCF events, no MCF event appears (Fig. 6). The cumulative number of LCF events (Figs. 2d and 3d) and deformation (Figs. 2c and 3e) recorded at LCF events shows a precursory trend as it evolves to an MCF event. For an ideal continuous system with an infinite number of meso-elements, the rate $\Delta u_{LCF}/\Delta U$ (or $\Delta N_{LCF}/\Delta U$) continuously and smoothly evolves to a singularity as it approaches the MCF point because an infinitesimal increment of U will result in a series of LCF events. Thus, the rate $\Delta u_{LCF}/\Delta U$ (or $\Delta N_{LCF}/\Delta U$) exhibits an accelerating trend as it approaches the singular point.

It can be seen that at the catastrophic failure point $dR/d\lambda$ tends to a singularity and thus $d\lambda/dR$ tends to zero. In this, R represents the "response quantity" directly related with the catastrophic event at the corresponding scale and λ represents the "load controlling variable", such as the boundary displacement U in the present model and λ_F is its value at the catastrophic point. In the vicinity of the point of catastrophic failure, if $d\lambda/dR$ can be approximately expressed as an *n-th* order infinitesimal of $(\lambda_F\text{-}\lambda)$, i.e. the limit of $d\lambda/dR/(\lambda_F\text{-}\lambda)^n$ tends to a finite quantity C, then $d\lambda/dR = C(\lambda_F\text{-}\lambda)^n$. Thus, $dR/d\lambda$ represents a power law accelerating trend

$$dR/d\lambda = C^{-1}(\lambda_F - \lambda)^{-\beta} \tag{4}$$

with λ approaching to λ_F. Where $\beta = 1/n$.

5 Conclusions

Our multiscale model successfully reproduces catastrophic events at different scales by representing the underlying physics of multiscale catastrophic events. The proposed methodology gives accurate results of the failure process driven only by a monotonically increasing boundary displacement. Small catastrophic (SCF) events appear both before and after the maximum load point on the macroscopic system. An SCF event occurring at small scale is driven by the local energy release from the corresponding elastic environment. This small event induces a clear jump in the local (and measurable) response driven by the progressive break of fibers in the meso-element, but leads to a much smaller (or immeasurable) fluctuation in the trend of the global response. Thus a small catastrophic failure (SCF) event may be observed locally but may not be available as a recordable precursory signal at the scale of the full system.

At the point of macroscopic catastrophic failure (MCF), the energy release from the system is sufficient to drive the failure process. Thus, a monotonic increase in the controlling variable leads to a disproportionate increase in the response quantities due to the coalescence of individual breakage events. For an ideal continuous system with an infinite number of elements, an infinitesimal increment of the controlling variable will result in a finite increment of the response quantities. This mechanism hosts a singularity precursor of the relative increase of response quantities with respect to the controlling variable.

In a multiscale system, failure is able to evolve across various length-scales. An LCF event can be driven by combining energy release from elastic springs at different scales. The coalescence of LCF events forms a macroscopic catastrophic failure (MCF) event. Thus, only the cumulative rates of LCF events, but not all events, exhibit a power law precursory trend accelerating to a singularity as it approaches its catastrophic point. This is because the much smaller events do not present a critical trend as the system approaches the catastrophic point – and a precursory signature is therefore not visible. This implies that it is crucial to recognize and distinguish effective precursors from monitoring signals that may be relevant to different scales. This is a key for the robust prediction of these events, and may be a possible cause that no obvious accelerating precursory signal is observed in advance of some large catastrophic events.

Acknowledgements This work is supported by National Natural Science Foundation of China (Grant No. 11672258) and Natural Science Foundation of Hebei Province (Grant No. D2020203001).

Compliance with ethical standards

Conflict of interest The authors declare no competing financial interests.

References

Bell AF, Naylor M, Heap MJ, Main IG (2011) Forecasting volcanic eruptions and other material failure phenomena: an evaluation of the failure forecast method. Geophys Res Lett 38(15):L15304

Boué A, Lesage P, Cortés G, Valette B, Reyes-Dávila G (2015) Real-time eruption forecasting using the material Failure Forecast Method with a Bayesian approach. J Geophys Res 120(4):2143–2161

Cornelius RR, Scott PA (1993) A materials failure relation of accelerating creep as empirical description of damage accumulation. Rock Mech Rock Eng 26:233–252

Cornelius RR, Voight B (1995) Graphical and PC-software analysis of volcano eruption precursors according to The Materials Failure Forecast Method (FFM). J Volcanol Geotherm Res 64:295–320

Duxbury PM, Beale PD, Moukarzel C (1995) Breakdown of two-phase random resistor networks. Phys Rev B 51:3476–3488

Griffith AA (1921) The phenomena of rupture and flow in solids. Philos Trans R Soc London 221:163–198

Hao SW, Liu C, Lu CS, Elsworth D (2016) A relation to predict the failure of materials and potential application to volcanic eruptions and landslides. Sci Rep 6:27877

Hao SW, Yang H, Elsworth D (2017) An accelerating precursor to predict "time-to-failure" in creep and volcanic eruptions. J Volcanol Geotherm Res 343:252–262

Hao SW, Yang H, Liang XZ (2017) Catastrophic failure and critical scaling laws of fiber bundle material. Materials 10(5):515–614

Hao SW, Zhang BJ, Tian JF, Elsworth D (2014) Predicting time-to-failure in rock extrapolated from secondary creep. J Geophys Res Solid Earth 119(3):1942–1953

Hao SW, Rong F, Lu MF, Wang HY, Xia MF, Ke FJ, Bai YL (2013) Power-law singularity as a possible catastrophe warning observed in rock experiments. Int J Rock Mech Min Sci 60:253–262

Heap MJ, Baud P, Meredith PG, Vinciguerra S, Bell AF, Main IG (2011) Brittle creep in basalt and its application to time-dependent volcano deformation. Earth Planet Sci Lett 307(1–2):71–82

Hidalgo RC, Kun F, Herrmann HJ (2002) Creep rupture of viscoelastic fiber bundles. Phys Rev E 65:032502

Jaeger JC, Cook NGW, Zimmerman RW (2007) Fundamentals of rock mechanics, 4th edn. Blackwell Publishing Ltd, Oxford

Kadar V, Kun F (2019) System-size-dependent avalanche statistics in the limit of high disorder. Phys Rev E 100:053001

Kilburn CRJ, De Natale G, Carlino S (2018) Progressive approach to eruption at Campi Flegrei caldera in southern Italy. Nat Commun 8:15312

Kilburn CRJ (2003) Multiscale fracturing as a key to forecasting volcanic eruptions. J Volcanol Geotherm Res 125:271–289

Kilburn CRJ (2012) Precursory deformation and fracture before brittle rock failure and potential application to volcanic unrest. J Geophys Res 117:B02211

Kilburn CRJ, Petley DN (2003) Forecasting giant, catastrophic slope collapse: Lessons from Vajont, northern Italy. Geomorphology 54(1–2):21–32

Kilburn CRJ, Voight B (1998) Slow rock fracture as eruption precursor at Soufriere Hills, volcano, Montserrat. Geophys Res Lett 25(19):3665–3668

Kun F, Hidalgo RC, Herrmann HJ, Pal KF (2003) Scaling laws of creep rupture of fiber bundles. Phys Rev E 67:061802

Lavallée Y, Meredith PG, Dingwell DB, Hess KU, Wassermann J et al (2008) Seismogenic lavas and explosive eruption forecasting. Nature 453(7194):507–510

Main IG (1999) Applicability of time-to-failure analysis to accelerated strain before earthquakes and volcanic eruptions. Geophys J Int 139:F1–F6

Main IG (2000) A damage mechanics model for power-law creep and earthquake aftershock and foreshock sequences. Geophys J Int 142:151–161

Main IG, Naylor M (2012) Extreme events and predictability of catastrophic failure in composite materials and in the Earth. Eur Phys J Special Topics 205:183–197

Mogi K (1995) Earthquake prediction research in Japan. J Phys Earth 43:533–561

Moreno Y, Gómez JB, Pacheco AF (2000) Fracture and second-order phase transitions. Phys Rev Lett 85(14):2865–2868

Naimark OB (2004) Defect induced transitions as mechanisms of plasticity and failure in multifield continua. In: Capriz G, Mariano P (eds) Advances in multifield theories of continua with substructure. Birkhauser Inc, Bostons, pp 75–114

Naimark O (2017) Criticality of Damage-Failure Transition in Quasi-Brittle Materials Under Dynamic and Shock Wave Loading. In: Ben-Dor G et al (eds) 30th International Symposium on Shock Waves 2. Springer International Publishing AG, Cham, pp 907–912

Naimark OB, Uvarov SV (2004) Nonlinear crack dynamics and scaling aspects of fracture (experimental and theoretical study). Int J Fract 128:285–292

Nechad H, Helmstetter A, El Guerjouma R, Sornette D (2005) Creep ruptures in heterogeneous materials. Phys Rev Lett 94:045501

Peirce FT (1926) Tensile Tests for Cotton Yarns V, 'the Weakest Link' Theorems on Strength of Long and Composite Specimens. J Textile Inst 17:T355–T368

Petley DN, Higuchi T, Petley DJ, Bulmer MH, Carey J (2005) Development of progressive landslide failure in cohesive materials. Geology 33(3):201–204

Pradhan S, Hansen A, Chakrabarti BK (2010) Failure Processes in Elastic Fiber Bundles. Rev Mod Phys 82:499–555

Salamon MDG (1970) Stability, instability and design of pillar workings. Int J Rock Mech Min Sci 7(6):613–631

Sornette D (1989) Elasticity and failure of a set of elements loaded in parallel. J Phys A 22(6):L243–L250

Sornette D (2002) Predictability of catastrophic events: Material rupture, earthquakes, turbulence, financial crashes, and human birth. Proc Natl Acad Sci USA 99(Suppl 1):2522–2529

Turcotte DL, Newman WI, Shcherbakov R (2003) Micro and macroscopic models of rock fracture. Geophys J Int 152:718–728

Vasseur J, Wadsworth FB, Heap MJ, Main IG, Lavallée Y, Dingwell DB (2017) Does an inter-flaw length control the accuracy of rupture forecasting in geological materials? Earth Planet Sci Lett 475:181–189

Vasseur J, Wadsworth FB, Lavallée Y, Bell AF, Main IG, Dingwell DB (2015) Heterogeneity: The key to failure forecasting. Scientific Reports 5:13259

Voight B (1988) A method for prediction of volcanic eruptions. Nature 332:125–130

Voight B (1989) A relation to describe rate-dependent material failure. Science 243:200–203

Voight B, Cornelius RR (1991) Prospects for eruption prediction in near real-time. Nature 350:695–698

Xue J, Hao SW, Wang J, Ke FJ, Lu CS, Bai YL (2018) The Changeable Power Law Singularity and its Application to Prediction of Catastrophic Rupture in Uniaxial Compressive Tests of Geomedia. J Geophys Res Solid Earth 123(4):2645–2657

Zapperi S, Vespignani A, Stanly HE (1997) Plasticity and Avalanche Behavior in Microfracturing Phenomena. Nature 388:658–666

Zhou SJ, Hao SW, Elsworth D (2018) Magnitude and variation of the critical power law exponent and its physical controls. Physica A 510:552–557